Scaling and stochastic cascade properties of NEMO oceanic simulations and their potential value for GCM evaluation and downscaling

Sébastien Verrier, Michel Crépon, Sylvie Thiria

AGU PUBLICATIONS

JGR

Journal of Geophysical Research: Oceans

RESEARCH ARTICLE

10.1002/2014JC009811

Key Points:
- Multiscale analysis methods are applied to NEMO OGCM simulations
- Several NEMO oceanic variables follow multifractal laws
- These laws should be useful for OGCM evaluation/downscaling

Correspondence to:
S. Verrier,
svlod@locean-ipsl.upmc.fr

Citation:
Verrier, S., M. Crépon, and S. Thiria (2014), Scaling and stochastic cascade properties of NEMO oceanic simulations and their potential value for GCM evaluation and downscaling, *J. Geophys. Res. Oceans*, *119*, 6444–6460, doi:10.1002/2014JC009811.

Received 15 JAN 2014
Accepted 12 AUG 2014
Accepted article online 14 AUG 2014
Published online 24 SEP 2014

Scaling and stochastic cascade properties of NEMO oceanic simulations and their potential value for GCM evaluation and downscaling

Sébastien Verrier[1,2], Michel Crépon[1,2], and Sylvie Thiria[1,2]

[1]Sorbonne Universités, UPMC Univ Paris 06, LOCEAN/IPSL, F-75005, Paris, France, [2]LOCEAN UMR7159 CNRS/IRD/MNHN, Paris, France

Abstract Spectral scaling properties have already been evidenced on oceanic numerical simulations and have been subject to several interpretations. They can be used to evaluate classical turbulence theories that predict scaling with specific exponents and to evaluate the quality of GCM outputs from a statistical and multiscale point of view. However, a more complete framework based on multifractal cascades is able to generalize the classical but restrictive second-order spectral framework to other moment orders, providing an accurate description of probability distributions of the fields at multiple scales. The predictions of this formalism still needed systematic verification in oceanic GCM while they have been confirmed recently for their atmospheric counterparts by several papers. The present paper is devoted to a systematic analysis of several oceanic fields produced by the NEMO oceanic GCM. Attention is focused to regional, idealized configurations that permit to evaluate the NEMO engine core from a scaling point of view regardless of limitations involved by land masks. Based on classical multifractal analysis tools, multifractal properties were evidenced for several oceanic state variables (sea surface temperature and salinity, velocity components, etc.). While first-order structure functions estimated a different nonconservativity parameter H in two scaling ranges, the multiorder statistics of turbulent fluxes were scaling over almost the whole available scaling range. This multifractal scaling was then parameterized with the help of the universal multifractal framework, providing parameters that are coherent with existing empirical literature. Finally, we argue that the knowledge of these properties may be useful for oceanographers. The framework seems very well suited for the statistical evaluation of OGCM outputs. Moreover, it also provides practical solutions to simulate subpixel variability stochastically for GCM downscaling purposes. As an independent perspective, the existence of multifractal properties in oceanic flows seems also interesting for investigating scale dependencies in remote sensing inversion algorithms.

1. Introduction

The dynamical properties of the ocean are of fundamental interest in geophysics and climate science. Since the oceans cover the three quarters of the earth surface, are a few kilometers deep and exchange many heat and gas fluxes with the atmosphere, they play a key role in the variability of climate. The horizontal and vertical motions of oceanic flows also largely govern the spatial distribution of phytoplankton, which is the basis of the oceanic biosphere. However, a key point about oceanic motions is their turbulent character. Last decades, it has been realized that mesoscale eddies (50–300 km) are very important in the spatial distribution of kinetic energy [e.g., *Semtner and Mintz*, 1977; *Richardson*, 1983; *Wyrtki et al*., 1976; *Krauss and Käse*, 1984]. Even though metrics such as the first internal Rossby radius may be used to characterize their size, the problem is more involved since these structures also transfer their energy to smaller ones, and so on. Submesoscale eddies and filaments are also dynamically important and their role should not be neglected [*Lévy et al*., 2010, 2012].

Numerical tools are indispensable for investigating turbulence in the ocean. The numerical approach consists to solve the numerical equations of motion (momentum equation, conservation of mass and of tracers concentrations) over a three-dimensional spatial grid. These equations are generally simplified with some hypotheses. Often numerical models of the ocean (hereafter OGCM) are based on the formulations of the so-called primitive equations [*Bryan*, 1969], but other formulations remain possible. In the general case, the approach is attractive due to its strongly physical formalism and has proven its utility both for the

understanding and forecasting of oceanic flows, including climate-related applications. The drawbacks of the approach are the large computational cost that limits available resolutions, and the problem of unresolved scales that is the consequence of the latter scale truncations. The first issue is partially addressed with the help of permanent improvements of the efficiency of (super)computers. However, resolutions are often limited to O(10 km) for global OGCMs even with a huge computational power. The problem of unresolved scales is tackled with the help of a parameterization, which generally involves some kind of diffusive operators [e.g., *Smagorinsky*, 1963; *Basdevant and Sadourny*, 1983; *Redi*, 1982; *Gent and Mcwilliams*, 1990; *Le Sommer et al*., 2011]. Nevertheless, this diffusion may also filter too strongly scales close to the grid spacing, leading to coarser effective resolutions for OGCMs that can be of the order of 2–10 times the grid step [*Skamarock*, 2004; *Lévy et al*., 2012].

A complementary approach would be to use statistical tools to characterize the variability of the different oceanic fields. However, since the variability is governed by turbulent processes, it has inhomogeneous and scale-dependent properties. For instance, the variance of a turbulent field strongly depends on the time and space scale at which it is estimated.

The correct approach for describing statistical properties of turbulent flows over a wide range of scales is to express statistics as function of the scale and of scale-independent exponents. This approach is fully consistent with classical theoretical works in statistical mechanics of turbulence. It is well known that in the inertial range, energy spectra of 3-D isotropic homogeneous turbulence should follow a $k^{-5/3}$ power law, where k is the spatial wave number [*Kolmogorov*, 1941], and that passive tracers concentrations should follow similar laws [*Obukhov*, 1949; *Corrsin*, 1951]. Many variants of these theories have been proposed to take into account the stratification of atmospheric and oceanic flows involving a few scaling ranges with $-5/3$ or -3 scaling exponents [e.g., *Charney*, 1971; *Lapeyre and Klein*, 2006]. Such scaling properties of spectra (with possibly different scaling exponents) have been observed over multiple dynamic (reference) and biological fields [e.g., *Currie and Roff*, 2006]. Spectra are also appropriate for statistical evaluation of a given data set: for instance, if the scaling law is replaced at the highest wave numbers by a flat curve of constant power, this is the indicator of a high level of white noise that contaminates high frequencies and reduces the effective resolution of the data. In a converse manner, when the spectra unexpectedly drops off at high frequencies with very high spectral exponent, this shows a lack of variability with excessively smooth data at small scales. Spectral analysis is useful to determine the effective resolution of an OGCM, which is the scale at which the spectra drops from the theoretical power law [*Skamarock*, 2004; *Capet et al*., 2008; *Lévy et al*., 2012]. Such applications are attractive since they combine the two approaches (numerical and statistical) in the modeling of oceanic variability over a wide range of scales. Such tools are therefore appropriate for the evaluation of oceanic (and atmospheric) oceanic models.

However, it is perhaps not always fully realized that spectra can only provide a truncated view of the overall multiscale variability of oceanic (and atmospheric) flows. This is due to that spectra are a statistical moment of the second order, i.e., a quantity that depends on, but does not characterize the probability distribution (the same remark applies to correlations and covariances). Even though for Gaussian random variables the knowledge of the mean and of the variance is sufficient to know the whole probability distribution, the problem is that variables of interest are generally non-Gaussian in geosciences. What is needed is therefore a tool that can deal with the changes in probability distributions over a wide range of scales. This has led to consider more sophisticated statistical approaches that deal with moments of multiple orders over a scaling range: these are multifractal approaches [e.g., *Schertzer and Lovejoy*, 1987] that are fully consistent with refined phenomenologies of turbulence where energy dissipation rates are not considered homogeneous but distributed over fractal sets by cascade processes [*Kolmogorov*, 1962; *Yaglom*, 1966]. In particular, spectral power laws are a particular (second order) consequence of multifractality in this framework.

The multifractality (in the time or space domain) of several oceanic fields (temperature, chlorophyll concentration) has been established by various studies based on in situ [*Seuront et al*., 1996a, 1996b, 1999] or remotely sensed from aircraft or satellite [*Lovejoy et al*., 2001; *de Montera et al*., 2011]. Therefore, it is very likely that if OGCMs outputs are statistically realistic (as suggested by spectral analysis) over a wide range of scales, then they also should follow multifractal statistics, for dynamic and tracers fields (velocity, sea surface temperature, height, and salinity). Moreover, it has recently been shown that the atmospheric counterparts of OGCMs indeed follow multiscale statistics conform to the predictions of the multifractal framework: *Stolle et al*. [2009] analyzed outputs of the GEMS and GFS meteorological model and from ERA-40 reanalysis and

found evidence of multifractal scaling laws extending from planetary scales to spatial scales of the order of 1°. *Gires et al*. [2011] also shown that rainfall products of nonhydrostatic regional Meso-NH model followed scaling and multifractal laws over meso and submesoscale regimes. Since the dynamical core of OGCMs is strongly analog to that of atmospheric models, we should expect to find similar results in oceanic models. However, there is almost no information available in the literature about the possible multifractality of OGCMs outputs. This is a limitation of existing statistical evaluation studies, which should be overpassed with the help of existing, well-established multifractal analysis techniques.

In the present study, we apply multifractal analysis tools to oceanic simulations provided by idealized regional configurations of the NEMO (Nucleus for European Modeling of the Ocean) [*Madec and The NEMO Team*, 2008] OGCM. This study is based on theoretical simulations of the dynamics starting from rest and not on analyses or reanalysis of real oceanic states. This permits to focus on the multiscale statistics of outputs produced by the dynamical core of NEMO regardless to corrections applied by data assimilation procedures. Such a methodology is useful for the evaluation of the core of the OGCM, but may of course be adapted if necessary to the study of realistic simulations, possibly including more complex boundary conditions.

Now let us present the outline of the study. In section 2, we propose a review on important concepts of the multifractal formalism. Some results of the literature related to oceanic fields are also synthesized in section 3. In section 4, we present our simulations based on the NEMO code. The monofractal analysis (based on first-order Kolmogorov structure functions) of the simulations is performed in section 5. Then, we move in section 6 on the multifractal analysis of multiple surface fields (SST, SSS, and velocity) produced by the model. Finally, we expose the potential implications of oceanic multifractality from a GCM and remote sensing perspective in section 7 and we conclude in section 8.

2. Theoretical Notions on Scaling and Multifractals

2.1. KOC Approach and Cascades

Many scaling theories exist for turbulent fields [e.g., *Kraichnan*, 1967; *Leith*, 1968; *Charney*, 1971]. These theories are generally (at least qualitatively) inspired by some fundamental ideas tracing back to *Kolmogorov* [1941]. In particular, the latter derived a scaling law for velocity increments in homogeneous 3-D turbulence:

$$\Delta v \stackrel{d}{=} \varepsilon^{1/3}.\Delta x^{1/3} \tag{1}$$

where v is the velocity, ε the flux of energy, Δx the distance over which the velocity increment Δv is taken, and $\stackrel{d}{=}$ means equality in probability distribution.

A direct consequence of equation (1) is the famous $-5/3$ law in terms of turbulent kinetic energy spectrum:

$$E(k) \propto k^{-5/3} \tag{2}$$

where k is the spatial wave number.

Similar extensions of equations (1) and (2) hold for passive tracers concentrations [*Obukhov*, 1949; *Corrsin*, 1951]. As may be seen, all these laws depend on a single scaling exponent 1/3, which is a sign of monoscaling or "monofractality."

An important hypothesis in the initial Kolmogorov formulation is the homogeneity of the energy flux. Later, it has been realized that such a hypothesis was untenable and leaded to refined scaling laws, where ε was distributed inhomogeneously [*Kolmogorov*, 1962], especially by cascade processes [*Yaglom*, 1966]. The study of the latter led to the development of the theory of multifractal cascades [*Mandelbrot*, 1974; *Schertzer and Lovejoy*, 1987; *Meneveau and Sreenivasan*, 1987; *She and Leveque*, 1994; *Dubrulle*, 1994]. The cascade formalism relies on some fundamental assumptions, in particular the description of scale transfers of energy occurring over neighboring scales in an autosimilar way while some quantity Φ (e.g., energy flux, tracer variance flux) is generally conserved in statistical average:

$$\langle \Phi_\lambda \rangle = const \tag{3}$$

where λ is the resolution, defined by convention as the ratio of a conventional maximal (or external) scale and the size of the pixels on which data are sampled. (Multiplicative) Cascade processes are defined

recursively by a sequence of successive refinements of resolutions for constructing Φ. For example, for a resolution refinement of factor 2, the relation involves a multiplicative modulation:

$$\Phi_\lambda = \Phi_{\lambda/2}.\mu\varepsilon \tag{4}$$

where $\mu\varepsilon$ is a random variable that does not depend on the resolution nor of the position of the point in space. $\mu\varepsilon$ should also have a statistical mean equal to 1 in order to ensure (equation (3)).

2.2. Conservative and Universal Multifractals

Due to the scale independence of $\mu\varepsilon$, multiplicative cascades converge to multifractal fields for which statistical moments follow power laws of the resolutions with scaling exponents that depend on the particular statistics order (denoted q). Namely, a scale-dependent positive physical quantity Φ_λ is multifractal when:

$$\langle \Phi_\lambda^q \rangle \propto \lambda^{K(q)} \tag{5}$$

where $K(q)$ is a convex function of the noninteger, positive value of q [*Lovejoy and Schertzer*, 2013, Appendix 3A] and describes the whole spectrum of the scaling exponents of Φ_λ. From the Wiener theorem, it may be shown that the spectrum of a multifractal process with conservative means follows a decreasing power law of the form:

$$E_\Phi(k) \propto k^{-\beta} \tag{6}$$

where $\beta = 1 - \mathrm{K}(2)$.

This means that the scaling of a power spectrum is indeed an particular case of the multiscaling described by the function $K(q)$. Other special values should be mentioned, namely, $K(0) = 0$, and, due to equation (3), $K(1) = 0$.

In the general case, there are very few constraints on $K(q)$ (convexity and special values), which means that the knowledge of $K(q)$ would in principle require an infinity of parameters. However, continuous-in-scale (i.e., that involve a continuum of scales instead of the dyadic cascade structure assumed in equation (4)) cascade processes have log-infinitely divisible distributions that can be decomposed into a mixture of lognormal, log-compound Poisson, and log-Lévy distributions (Lévy-Khinchine theorem) [see, e.g., *She and Waymire*, 1995]. In special cases, $K(q)$ follows an analytical form that is even more easily parameterizable. Log-stable distributions have been a popular choice leading to the Universal Multifractal Model [*Schertzer and Lovejoy*, 1987, 1997]. The latter has been found suitable for the statistical modeling of multiple geophysical fields [*Lovejoy and Schertzer*, 2007], especially in atmospheric science [*Lovejoy and Schertzer*, 2010a, 2010b, 2010c], but also in oceanic science (e.g., references below).

Within, this universal framework, the moment scaling function is expressed as follows:

$$K(q) = \frac{C_1}{\alpha - 1}(q^\alpha - q) \tag{7}$$

which depends on two parameters, and obviously verifies the properties $K(0) = K(1) = 0$.

C_1 describes the inhomogeneity associated with intensity levels close to the mean field, it belongs to the real interval [0,D] where D is the dimension of the space over which the cascade is constructed. The parameter α has a (real) value in the range 0–2 and describes how quickly the inhomogeneity of the field changes when we are leaving away from the mean level. It is a multifractality parameter: while $\alpha = 0$ corresponds to a monofractal case with linear K(q), $\alpha = 2$ is a characteristic of lognormal multifractals.

2.3. Nonconservative Multifractals

A wider class of multifractal processes has also been defined in order to combine the initial Kolmogorov approach with the benefits of cascade refinements. These nonconservative multifractals rely on fractional integrations of real-order H of conservative multifractal cascades [*Schertzer and Lovejoy*, 1987]. Locally, these cascades correspond to the following equation relating the integrated observables Q to the cascade Φ:

$$\Delta Q \overset{d}{=} \Phi_\lambda.\Delta x^H \tag{8}$$

where ΔQ stands for absolute increments of Q over a distance Δx and H is a scaling parameter. This formulation is very similar to (equation (1)) (for which H = 1/3) and leads to a power law spectrum with an

exponent $\beta = 1 - K(2) + 2H$. Since the fractional integration corresponds to a low-pass filtering by k^{-H} in Fourier space, H may be viewed as a smoothing parameter. It is also a nonconservativity parameter in the sense that the mean of the absolute increments of a fractionally integrated process depends on Δx. From this property, H may be estimated by plotting the first-order structure function in log-log coordinates, where the function is defined as:

$$\langle |Q(x+\Delta x) - Q(x)| \rangle \propto |\Delta x|^H \tag{9}$$

The addition of a fractional integration to universal multifractals is called the Fractionally Integrated Flux (FIF) model [*Schertzer and Lovejoy*, 1987], which therefore depends on the three parameters H, α, C1.

3. Brief Overview of Scaling and Multifractality in Ocean Science

Many oceanic fields that have (or are distributed by) turbulent characteristics are expected to follow scaling and possibly multifractal properties. These include the velocity field, the passive tracers (potential temperature, potential salinity, sea surface temperature (SST) and salinity (SSS), chlorophyll concentration, and its surrogates such as fluorescence), and fields related by integrations or derivations to the velocity field (vorticity, sea surface height (SSH)) since integrations and derivations are themselves power law filterings in Fourier space. Investigations of spectral properties of dynamical and/or plankton-related fields have already been performed many times on both numerical simulations and observational data.

Spectral analysis of numerical simulations of oceanic variables (SST, surface currents and densities, but also variables in the interior of the ocean) has already been performed and reported in published studies [e.g., *Skamarock*, 2004; *Capet et al*., 2008; *Klein et al*., 2008; *Lévy et al*., 2012]. These works led to important conclusions about the multiscale behavior of OGCMs, especially (1) the existence of a power law scaling regime at scales much larger than the grid step; (2) the dependence of the spectral exponents on the depth (exponents often close to -2 at the surface and to ~ -3 below); (3) a limited effective resolution evidenced by a spectral drop at the higher frequencies.

Regarding data, there are also multiple results based on very different kinds of measurements. Spectral analysis of (airborne and spaceborne) remote sensing SST data has a long history [*Saunders et al*., 1972; *Holladay et al*., 1975; *Deschamps et al*., 1981]. More recently, well-known satellite SST products have also been analyzed [*Reynolds et al*., 2010], evidencing scaling regimes but also limitations at higher frequencies due signal processing artifacts. Altimetric measurements of sea surface height have also been considered by the literature, in particular, the works by *Stammer* [1997] and *Le Traon et al*. [2008]. Regarding biological data, there exists also multiple results mainly based on in situ time series [see, e.g., *Currie and Roff*, 2006, and references therein]. Spectra of biological data are nevertheless often more complex with several piecewise characteristics.

Multifractal analysis tools have widely been applied to in situ data, especially temperature and fluorescence time series (the latter being a surrogate of phytoplankton concentration) [*Seuront et al*., 1996a, 1996b, 1999]. The latter studies showed the existence of multifractal properties in the time domain in several scaling regimes. For most fields, a more or less common set of universal multifractal parameters is $\alpha \sim 1.7$, C1 = 0.03–0.05, H = 0.3–0.4, with significant exceptions (e.g., "biologically active" fluorescence was characterized by much lower values of α and H, and Lagrangian (drifter) data were associated with higher values of H). *Seuront et al*. [1999] also demonstrate the existence of multifractal properties for the in situ salinity, with multifractal scaling parameters that are remarkably consistent with those of the temperature.

Then, *Lovejoy et al*. [2001] investigated the horizontal scaling properties of remote sensed ocean color data collected by airborne sensors. They showed that radiances in eight (visible and IR) channels were scaling in the range 100 km–100 m with parameters $\alpha \sim 2$, C1 ~ 0.05, H ~ 0.2. Recently, the multifractality of chlorophyll concentrations in the space domain was assessed by *de Montera et al*. [2011] based on chlorophyll data products based on SeaWifs satellite measurements. In the latter case, the scaling held in the range 128 km–4 km with multifractal exponents values $\alpha \sim 1.9$, C1 ~ 0.1, H ~ 0.4 which are rather similar to parameters usually found in atmospheric science for several dynamical and tracers fields [e.g., *Lovejoy and Schertzer*, 2010a, 2010b, 2010c].

Other important works investigated the multifractality of remote sensing SST and surface chlorophyll concentration products [*Isern-Fontanet et al*., 2007; *Nieves et al*., 2007; *Turiel et al*., 2008, 2009], although with

Table 1. Details of the NEMO Simulations and Physical Assets

Configuration	GYRE	BJET
Resolution	1/9°	5 km
Diffusion operator	Bilaplacian	Bilaplacian
Viscosity	$-1.0e+10$ m^4/s	$-7.8e+8$ m^4/s
Diffusivity	$-1.0e+10$ m^4/s	$-2.0e+8$ m^4/s
Boundary	Free slip	Zonally periodic and free slip
Max scale	3000 km	2000 km
Grid size	$272 \times 182 \times 31$	$400 \times 100 \times 80$
Tra	Pot temperature and salinity	Potential density
Equation of state	Linear	Salinity = constant
Zonal nudging	False	True
Spin-up window	50 years	1 year
Study window	1 year	1 year
Sampling in study window	2/month	6/month
Time step	900 s	300 s
Wind forcing	GYRE analytical forcing (sbcgyre)	Constant

the help of the slightly different formalism of singularity exponents. These authors found evidence of multifractal properties that can even be used for estimating high-quality maps of streamlines. Moreover, the same team recently found that SST and SSS are likely to share a common multifractal structure [*Umbert et al*., 2014].

These results are significant evidence of the existence of multifractal properties emerging in ocean dynamics and biological fields. Such properties indeed need to be verified on numerical simulations of oceanic GCM outputs, which is missing in the literature (excepted, on one hand, the paper by *Umbert et al*. [2014] who analyzed products that include data assimilation, and, on the other hand, a study carried out at LOCEAN/IPSL by *de Montera et al*. [2011]) while their atmospheric counterparts have recently been analyzed successfully within this framework. In particular, *Stolle et al*. [2009] analyzed the cascade structure of fluxes derived from meteorological forecasting GCMs and reanalyzes and found multifractal cascade properties extending from planetary and synoptic scales to approximately 1° space scale, with multifractal exponents $\alpha \sim 1.6$–2, C1 ~ 0.05–0.1 for most atmospheric state variables. The latter study has been confirmed and extended by *Lovejoy and Schertzer* [2011] based on ECMWF reanalyses. These authors also provided estimates of the H parameter in horizontal directions but found more nonstandard parameters and evidence the importance of horizontally anisotropic properties of the flows.

4. Simulation Setup

NEMO [*Madec et al*., 1998; *Madec and The NEMO Team*, 2008], standing for "Nucleus for European Modeling of the Ocean," is a primitive equation oceanic numerical model that can be adapted in a variety of global (ORCA) or regional (GYRE,. . .) configurations of various resolutions. NEMO (and its direct predecessor OPA) has been the basis of many studies in physical oceanography [e.g., *Madec et al*., 1996; *Aumont et al*., 1998; *Marchesiello et al*., 2011; *Lévy et al*., 2010, 2012] and includes components for the dynamics (OPA), sea-ice (LIM), biology (PISCES), data assimilation, etc. [*Madec and The NEMO Team*, 2008]. In this study, we focus on an idealized reference configuration called GYRE with flat bottom and "vertical walls" boundary conditions and with specific analytical wind forcings. A linear equation of state describes relationships of the density, the temperature, and the salinity. The configuration is supposed to be representative of the Gyre circulation in the Northern Atlantic. The domain (of dimension O(3000 $\times$ 2000 km)) is defined on rotated axes [*Hazeleger and Drijfthout*, 1998] and a beta-plane approximation is used. While the configuration was originally defined on a 1° grid, it may be easily extended to higher spatial resolutions.

In the present study, we have performed simulations of the dynamical fields NEMO-GYRE at 1/9° (272×182 pixels in the horizontal) with 31 vertical levels (with an increased resolution near to the surface), starting from rest initial conditions. The state variables are the horizontal components of the velocity, the temperature, the salinity, and the SSH. Physical choices (turbulence closures, boundary conditions) are summed up in Table 1. Turbulence closure is needed in every GCM and since the problem is globally unsolved, the performance of subgrid parameterization may impact the model outputs even at the scales greater than the

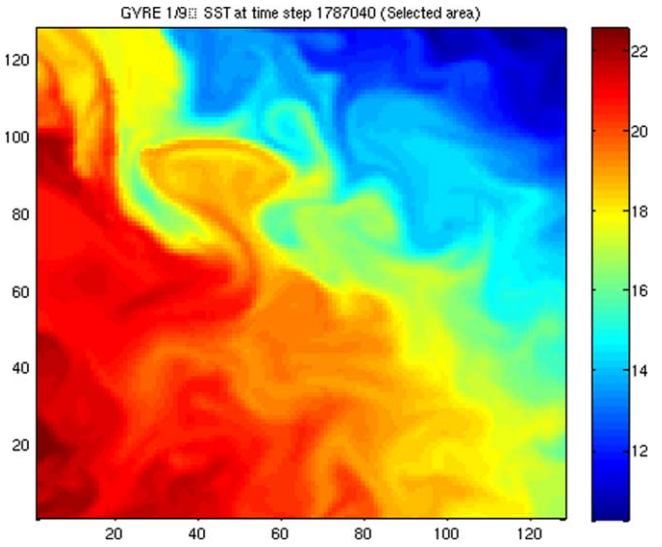

Figure 1. Snapshot of the sea surface temperature field produced by NEMO-GYRE 1/9° at time step 1,787,040. The area shown corresponds to the square area selected for multifractal analysis.

grid step. This typically causes problems of "effective resolution" that are significantly greater than the grid step. In our simulations, a horizontal bi-Laplacian scheme was used due to its scale selectivity, thus favoring initiation of turbulence which is strongly filtered out by, e.g., Laplacian operators [*Griffies and Hallberg*, 2000]. The values of viscosities and diffusivities have been chosen with respect of the values proposed by *Lévy et al*. [2012] with slight adaptations. Since it may take some time to reach a strongly turbulent state from rest (and especially at significant depth), we performed a spin-up simulation representative of 50 years of flow, with time step 900 s. A snapshot of the SST surface field (in a selected square area) after the spin-up time is given in Figure 1. We notice strong velocities in the western part of the figure, as the meandering of surface temperature structures, coherently with the high-resolution simulations by *Lévy et al*. [2012].

We also considered dynamical simulations performed in a different configuration of NEMO called BJET. This configuration, derived from the more well-known EEL configuration, is set over a 2000 × 500 km region with zonally periodic boundary conditions with axis parallel to the north-south and east-west directions. Idealized bottom boundary conditions apply (as in the GYRE case) and at the surface forcings are assumed to be representative of a midlatitude region. In this configuration, the salinity is fixed as a constant at 35 psu and the passive scalar is potential density. Initial conditions are at rest and defined from stratified initial conditions in density and temperature, permitting the generation of a zonal jet. By construction, the BJET configuration includes a perturbation of the initial state designed to generate a baroclinic instability that destabilize the zonal jet centered in the domain and produces turbulent motions. By construction, generation of turbulent motions is quicker in BJET than in the GYRE configuration. We performed a BJET simulation representative of 2 years at 5 km resolution with time step 300 s. The first year is the spin-up of the simulation while the second year is devoted to the statistical study. Due to the choice of the resolutions, the grids are of dimension 400 × 100 × 80. As shown on the snapshot (Figure 2), the zonal jet destabilization is associated with a zone of meso and submesoscale eddies.

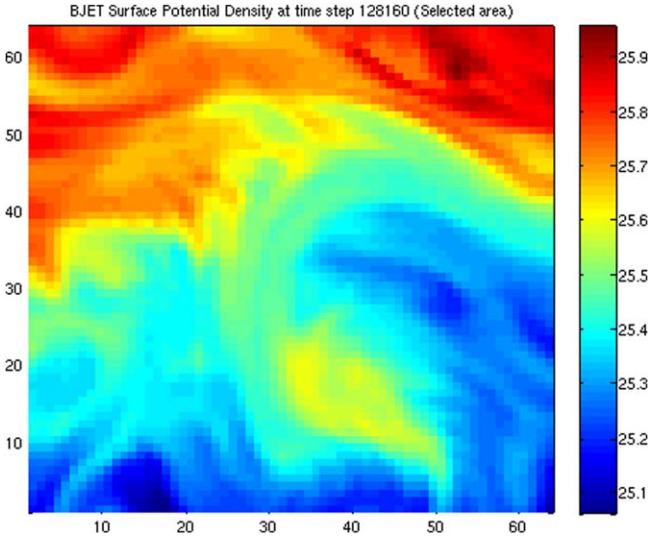

Figure 2. Snapshot of the surface density field produced by NEMO-BJET 5 km at time step 128,160. The area shown corresponds to the square area selected for multifractal analysis.

The spin-up simulations were then followed by subsequent simulations performed from restart files produced at the end of the spin-up window. The additional time-window considered was of 1 year in both cases with six backup restart files per month in the BJET case and two per month in the GYRE simulation (note,

by convention we set up all "months" considered in this study to a 30 day duration for simplification in the GYRE case). Then we analyzed the surface fields stored in the 74 (resp. 25) restart files associated to each simulation, these fields are analyzed in the two next sections.

5. Structure Function Analysis of the Simulated Surface Fields

Outputs of (oceanic or atmospheric) GCM simulations are strongly anisotropic due to a strong meridional stratification. In the case of regional GCMs located in the midlatitudes, this stratification is monotonic and similar to an additional trend that should be removed before statistical analysis of the turbulent part of the field. Indeed, it is well known that the presence of trends in data may significantly affect the outputs of spectral analysis tools [*Skamarock*, 2004]. For this reason, we did not apply spectral analysis on the available data but focused on other mono and multifractal estimators. As noted by *Lovejoy and Schertzer* [2011], monofractal estimators applied directly on the GCM state variables may also produce questionable results in the presence of anisotropic fields. On the contrary, multifractal analysis of fluxes estimated by derivation of the state variables are not sensitive to these artifacts [*Stolle et al*., 2009; *Lovejoy and Schertzer*, 2011] since they remove any trend by construction, but there results are limited to the scaling properties of conservative fluxes, not of the physical fields themselves (see equation (8)). Analysis of the fluxes of NEMO simulations will be detailed in the next section.

Direct analysis of oceanic GCM physical variables (SST, SSS, SSH, velocity, etc.) is useful to estimate the multifractal exponent H defined in equation (8). We have chosen to estimate H directly from a first-order Kolmogorov structure function analysis which is based on the study of the scaling of mean increments of the field with respect to the distance (as expressed by equation (9)). Even though alternative definitions of structure functions do exist (e.g., Haar structure functions) [cf. *Lovejoy and Schertzer*, 2012], the classical definition based on equation (9) was kept due to its simplicity and its good performance for $0 < H < 1$.

From the NEMO simulations described in section 4, we extracted square maps centered in turbulent areas (for each state variable, we have 74 maps close to the jet center for BJET simulations; and 25 maps close to the north-western of the GYRE domain). It is obvious that structure functions are strongly sensitive to anisotropies in the field. In particular, the latitudinal stratification adds a trend to the data in the north-south direction. In order to avoid strong biases at large increments, such a trend has to be removed before computing the first-order structure functions (i.e., empirical averages of absolute increments, see equation (9)). Nevertheless, it is important to note that more subtle effects may also impact the scaling properties of the simulations, even after detrending. Indeed, zonal and meridional gradients are likely to be different physically and in some cases [*Lovejoy and Schertzer*, 2011] this could imply different values of H along different directions (e.g., east-west versus north-south). In the following, structure functions have been estimated along zonal and meridional directions.

Figures 3a–3d show an example of structure function obtained for SST, SSS, surface velocity data (GYRE), and potential density data (BJET). For most NEMO variables, these graphs show a rupture at O(5–10) times the grid step separating a large-scale regime, with a mean scaling exponent H = 0.2–0.4, from a small-scale regime with a steeper scaling, with H = 0.7–0.8, the detailed result being reported in Tables 2 and 3 (including the case of the BJET velocity, not shown in Figure 3). The large-scale exponent is coherent with classical values in geophysics: recalled that $H = 1/3$ corresponds approximately to the classical $-5/3$ turbulent spectral exponent. The result is also quite coherent with published spectral analyses of OGCM surface outputs, even though the latter results often favor a spectral exponent closer to -2, hence $H \sim 1/2$ [*Klein et al*., 2008; *Capet et al*., 2008; *Lévy et al*., 2012]. The dichotomy between the large-scale, turbulent, regime ($H \sim 1/3$ to 1/2) and a small-scale, smooth, regime (with H closer to 1 or k^{-3} power spectrum) has also been observed by the authors of the three papers cited above. The interpretation of the scale break and of the small-scale regime is likely to be related with the model hyperviscosity which still affects the smallest scales, e.g., a few times the grid step. In this case, this would mean that the effective resolution of the model could be significantly larger than the grid step. Nevertheless, we will see that such a scale break is not confirmed by multifractal analysis tools in the next section.

From Tables 2 and 3, it is apparent that in some scale ranges the estimate of H is quite sensitive to the direction considered. As shown in Figures 3a–3d and in the tables, H is slightly but sometimes significantly greater in the east-west direction compared to the North direction. This is especially the case

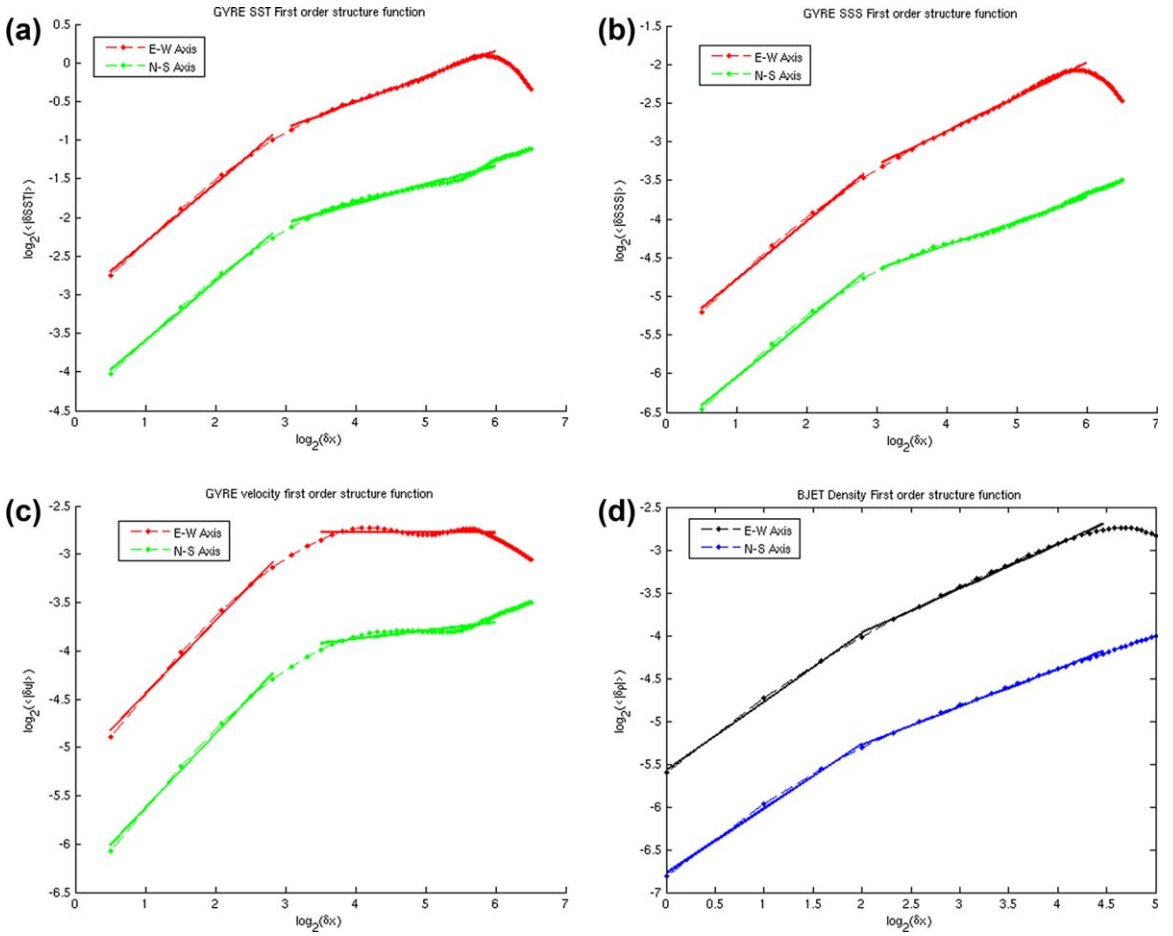

Figure 3. First-order structure functions in log2-log2 coordinates for the following surface variables in the analysis window: (a) GYRE 1/9° SST, (b) GYRE 1/9° SSS, (c) GYRE 1/9° zonal velocity, (d) BJET potential density. The fit regimes are detailed in Tables 2 and 3. The abscissa coordinate is associated to the lag δx expressed in number of gridsteps, with small scales on the left.

for the large-scale regime for GYRE SST and SSS fields where $H_{N\text{-}S} \sim H_{E\text{-}W} \times 0.7$. On the contrary, the estimate of H does not seem to depend on the direction in the small-scale regime (i.e., $<$90 km for the GYRE simulations). This small-scale isotropy could be related to the fact that the smaller scales are likely to be affected by the (isotropic) model horizontal diffusion.

Regarding the interpretation of large-scale exponents, it is worth pointing out that in a recent application of similar tools to atmospheric GCM outputs [*Lovejoy and Schertzer*, 2011], the authors found different exponents H along east-west and north-south directions and attributed the difference to an effect of the combination of important GCM properties, i.e., GCM (hyperviscosity-related) isotropy at small-scales and prescribed anisotropy at large scales. While similar ideas should apply to our results, there remain some

Table 2. Multifractal Scaling Regimes and Parameters for the BJET Simulation

Configuration	Number of Maps	Variable	Scaling Range (km)	H	α	C1
BJET5km	74 maps 64 × 64	Surface density	120–20	0.51 ± 0.02 (E–W) 0.44 ± 0.01 (N–S)		
BJET5km	74 maps 64 × 64	Surface density	20–5	0.80 (E–W) ± 0.13 0.76 (N–S) ± 0.17		
BJET5km	74 maps 64 × 64	Surface density	80–10		1.93	0.08
BJET5km	74 maps 64 × 64	Uzon	160–40	0.45	1.83	0.12
BJET5km	74 maps 64 × 64	Uzon	40–10	0.78	1.83	0.12

Table 3. Multifractal Scaling Regimes and Parameters for the GYRE Simulation

Configuration	Number of Maps	Variable	Scaling Range (km)	H	α	C1
GYRE1/9	25 maps 128 × 128	SST	500–90	0.32 ± 0.01 (E–W) 0.23 ± 0.02 (N–S)		
GYRE1/9	25 maps 128 × 128	SST	90–10	0.76 ± 0.10 (E–W N–S)		
GYRE1/9	25 maps 128 × 128	SST	750–20		1.82	0.10
GYRE1/9	25 maps 128 × 128	SSS	500–90	0.44 ± 0.01 (E–W) 0.31 ± 0.01 (N–S)		
GYRE1/9	25 maps 128 × 128	SSS	90–10	0.75 ± 0.10 (E–W) 0.73 ± 0.12 (N–S)		
GYRE1/9	25 maps 128 × 128	SSS	750–20		1.79	0.10
GYRE1/9	25 maps 128 × 128	Uzon	500–90	0.00 ± 0.01 (E–W) 0.09 ± 0.02 (N–S)		
GYRE1/9	25 maps 128 × 128	Uzon	90–10	0.75 ± 0.12 (E–W) 0.76 ± 0.12 (N–S)		
GYRE1/9	25 maps 128 × 128	Uzon	750–20		1.87	0.12

differences in the estimated exponents and in the nature of anisotropy since Lovejoy and Schertzer generally found greater exponents in the north-south direction.

Whatever possible problems involved by the detrending step, the results of this paragraph show clearly that the (piecewise) scaling properties of the observables always share the fundamental properties of integrated "nonconservative" fractal fields, i.e., $H > 0$. This means that these fields cannot be directly modeled by conservative multifractals (for which the spectral slope is $1 - K(2) < 1$). This is also the case of most atmospheric fields [*Lovejoy and Schertzer*, 2010a, 2010b, 2010c] and for most turbulent flows. However, for these fields, the conservative quantity that is directly cascaded is not the state variable field but a hidden (energy or variance) flux. This is coherent with the principle of theories of turbulent fields with heterogeneous, sparse energy fluxes (see theoretical remarks in *Lovejoy and Schertzer* [2010a, 2010b, 2010c]).

6. Multifractal Analysis of Conservative Fluxes Derived From Surface Maps

As explained above, fractionally integrated multifractal models presented in section 2.3 are likely to be necessary for representing most oceanic surface fields. Within this framework, we shall consider the superposition of an overall, fractional integration filter that strongly constrains the spectral shape and of a cascading quantity Φ, often called "flux" [*Lovejoy et al*., 2011], which is representative of sharp gradients (see equation (8)).

Then, we aim at assessing the assumed cascading structure of the fluxes. However, a classical difficulty at this step is to invert Φ from the observable variables. Theoretically, this would need a fractional derivative of order *H*, which is equivalent to a fractional integration of order *–H*. However, two problems arise in practice: *H* is always known within some uncertainty and the positivity of Φ is generally not respected from numerical differentiation of the observables. These kinds of difficulties have led to several solutions in the multifractal literature. One possibility is to use convenient wavelets to filter the signal [*Nieves et al*., 2007; *Turiel et al*., 2008], for instance using the wavelet-transform modulus-maxima method [*Muzy et al*., 1991, 1993].

However, most studies relying on the universal multifractal model used another simple solution, validated on analysis of multifractal fields [*Lavallée et al*., 1993; *Tessier et al*., 1993]. In this context, the processing is the following:

1. First differentiate the observed integrated field at an order > H. Generally, an integer order of differentiation is used. On 1-D, the classical choice is the finite difference increments while in 2-D a finite difference Laplacian performs well [*Tessier et al*., 1993]. It is important that the order of differentiation be greater than H since the statistical cascade structure is more affected by integrations than by overdifferentiations [*Lavallée et al*., 1993]. Another advantage of the Laplacian is its efficiency in removing trends.
2. Then take absolute values (and normalize by the mean) in order to get an estimate of Φ at the maximal available resolution λ_{max}.
3. Estimate Φ_λ at various resolutions by averaging contiguous pixels of the previous estimate $\Phi_{\lambda max}$.

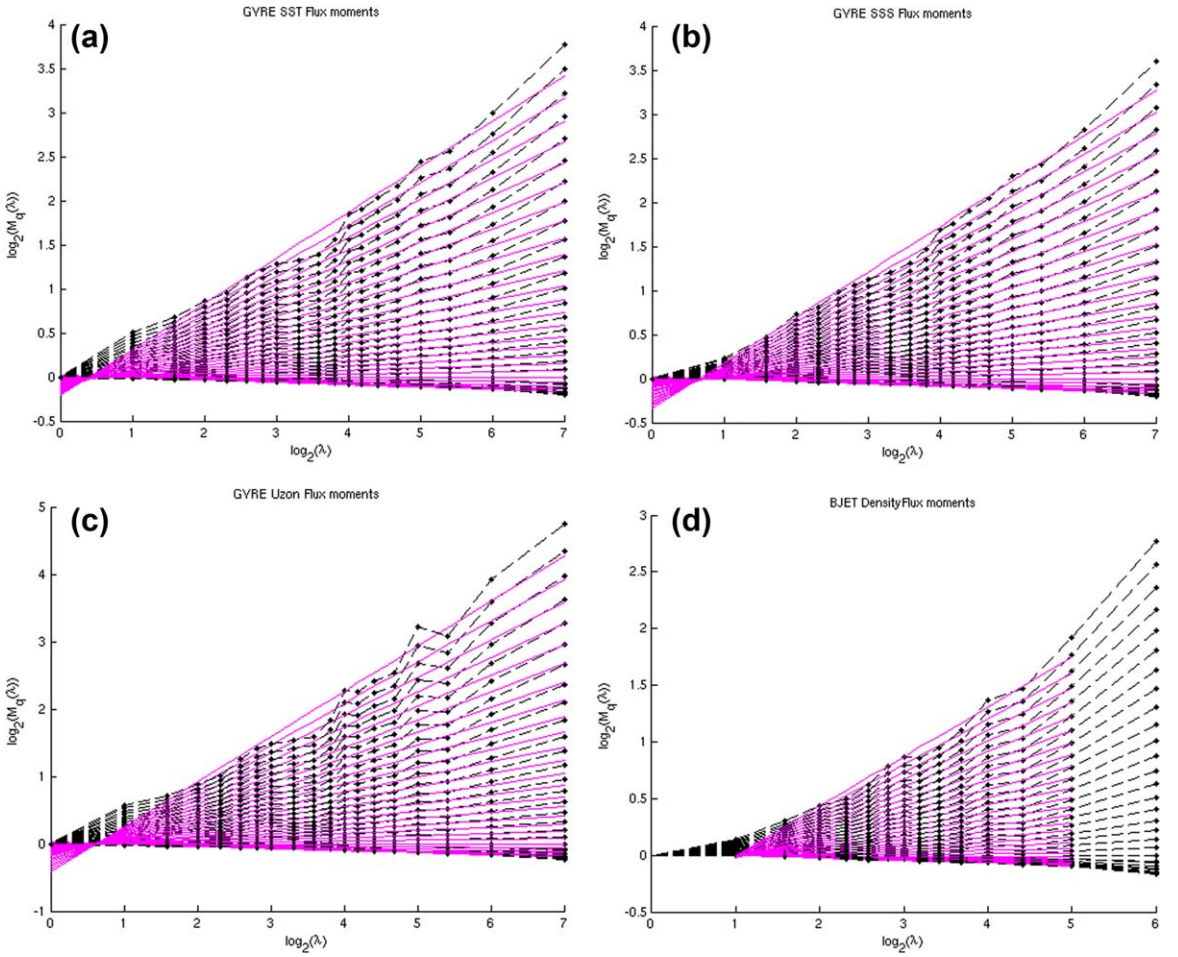

Figure 4. Fluxes empirical moments $M_q(\lambda)$=*empiricalmean*(Φ_λ^q) (orders q = 0. . .3) in log2-log2 coordinates for the following surface fields in the analysis window: (a) GYRE 1/9° SST, (b) GYRE 1/9° SSS, (c) GYRE 1/9° zonal velocity, (d) BJET potential density. The abscissa coordinate is the log2 of the resolution λ (λ = domain size/pixel size). Thus, large scales are on the left (x = 0 corresponds to the domain size, i.e., 1600 km for the GYRE subdomain considered in this study, Figures 4a–4c).

The latter methodology has been applied for the (undetrended) NEMO state variables considered in the previous section, leading to a multiscale estimate of the flux Φ_λ for each field. Then, statistical moments of the cascades are computed at various orders q such that we may investigate the validity of the fundamental equation of the multifractal formalism (equation (5)). The choice of the orders is important since a narrow range of moments reduces the information we get from the data (narrower family of scaling exponents), but a too large range may involve biased high-order estimates. Here the moment orders *q* are regularly sampled in the range 0–3 in order to avoid sampling/divergence problems arising for higher-order moments [e.g., *Lombardo et al*., 2013; *Schertzer et al*., 2013]. The results are plotted in Figures 4a–4d, which shows the moments as a function the resolution in log-log coordinates for each flux. As expected from equation (5), we may approximate the dependence of the statistics by power laws of the resolution with exponents K(q) that can be readily fitted by the linear regressions in Figures 4a–4d. It is remarkable that correct scaling laws are verified by most variables over almost all the available scale ranges which extend from 320 to 5 km for BJET simulations and from 1600 to 11 km for the GYRE simulations. The main limitations consist in some discrepancies at large scales close to the square domain size and in other slight discrepancies at small scales (smaller than 2 times the gridstep). Details on scaling ranges are reported in Tables 2 and 3. Despite these discrepancies, the scaling is generally proper for all oceanic variables considered and for all computed moment orders. Remarkably, we do not find any rupture in the scaling of the fluxes, which is an important difference between the results of the present section and the previous one. This means that even though the GCM state variables are partly filtered at small scales, the NEMO code is nevertheless able

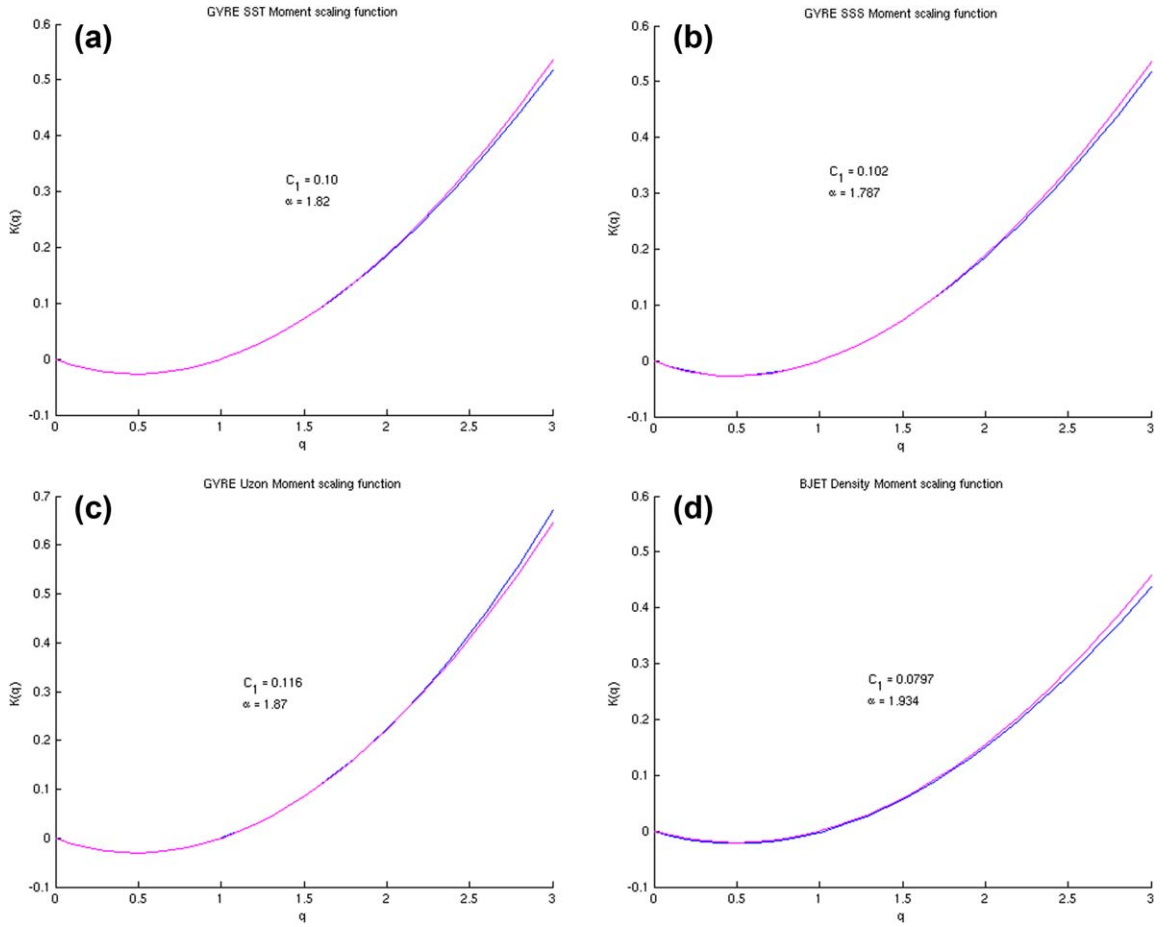

Figure 5. Moment scaling functions K(q) for the following surface variables in the analysis window: (a) GYRE 1/9° SST, (b) GYRE 1/9° SSS, (c) GYRE 1/9° zonal velocity, (d) BJET potential density. The empirical curve is drawn in blue, the theoretical fit (optimal close to q = 1) is drawn in pink.

to reproduce more correctly scaling properties of the fluxes down to the smallest resolved scales. The quality of the scaling of flux statistics is qualitatively comparable to that identified by *Stolle et al*. [2009] for AGCM outputs.

The scaling coefficients K(q) are plotted as a function of the order q (Figures 5a–5d). We added the graph of the least squares fit obtained from the universal parameterized form (equation (7)) (note that the fit was optimized for moments orders comprised between 0 and 2 in order to avoid possible sampling artifacts on higher-order moments). It may be seen from the quality of the fits that the two-parameter universal form performs well in describing the statistics of the field cascades. Combined with the previous results on H, this means that the FIF model defined in section 2.3 is able to describe the scaling of multiorder statistics of oceanic fields. All the multifractal parameters are reported in Tables 2 and 3—in particular, we found consistent multifractal parameterizations for SST and SSS fields, and for velocity fluxes with $\alpha \sim 1.8$ and $C1 \sim 0.1$. The parameters are more or less similar to those estimated from empirical oceanic data by various authors (as summarized in section 3). These multifractal exponents are also very comparable with those of atmospheric fluxes estimated on numerical AGCM outputs by *Stolle et al*. [2009] and *Lovejoy and Schertzer* [2011]. Finally, we should mention that our results on SST and SSS multifractal parameters are consistent with the works by *Umbert et al*. [2014] who found a common multifractal structure on SST and SSS products.

7. Additional Comments on Oceanic Multifractality and OGCMs

The previous sections have shown the existence of scaling and multifractal properties on NEMO oceanic simulations. We have also seen that qualitatively similar properties have already been found on many

oceanic in situ or remotely sensed measurements. This confirms that scaling and multifractals are a very convenient framework to understand the statistics of the oceanic variability over a wide range of scales. The present section aims at illustrating a bit more the potential interest of the framework for ocean modelers. Meteorological equivalents of some of these potential applications have recently been proposed in the literature.

7.1. OGCM Evaluation

A direct application of the formalism, illustrated by the present paper and by previous papers in atmospheric science [*Stolle et al*., 2009; *Lovejoy and Schertzer*, 2011], is the evaluation of the statistics of oceanic numerical models. Contrary to other existing statistical tools, multifractal analysis tools do not work at an arbitrary fixed scale but are able to investigate a wide range of scales. They are therefore able to:

1. Detect spurious breaks in the scaling due to incorrect physics: for instance, by using an overdiffusive physical scheme, we may spuriously wash out small-scale variability, which would lead to an overattenuation of high-order moments (and a spectral drop).
2. Intercompare the intermittency and variability of the outputs of two different GCMs. We may easily see whether a given GCM generates more scale-by-scale variability compared with one another, which could be compared with reference data/or reanalyses.
3. Deal simultaneously with different state variables: for instance, it may be seen if the model is better for simulating one variable but not one another.

7.2. Downscaling of Oceanic Fields

A direct application of the multifractal framework is downscaling which means inferring unaccessible or unresolved small-scale variability from low-resolution data or simulations. Due to the multiplicative structure of multifractal cascades (e.g., equation (4)), the stochastic generation of missing small-scale variability may be performed readily with the help of discrete or continuous in scale multifractals. Some example of multifractal downscaling of atmospheric fields (especially rainfall) have been recently been presented in the literature [*Rebora et al*., 2006; *Sharma et al*., 2007; *Onof and Arnbjerg-Nielsen*, 2009; *Gires et al*., 2012] generally based on discrete in scales conservative multiplicative cascades. However, in oceanography since most cascades include a strong fractional integration (as seen in sections 5 and 6), it would be questionable to retain such an artificial discretization of scales since the fractional integration operator is by itself continuous in scale. Nevertheless, as shown by *Verrier* [2011] we may get rid of conservativity and discrete scale hypotheses in downscaling algorithms. For nonconservative, continuous-in scale oceanic field, the main steps of the algorithm would be the following:

1. Inversion of the fractional integration (determining a positive flux with $H = 0$ from data characterized by $H > 0$).
2. Stochastic disaggregation of the flux with the help of conservative multiplicative cascades.
3. Adding a new fractional integration to estimate downscaled realizations of the field.

Figures 6a and 6b show an example of resolution enhancement of a detrended SST field produced by the NEMO-GYRE code using such a method. Of course, a single realization is shown but this methodology may produce an ensemble of possible disaggregated fields. The latter may have some interest for computing ensemble statistics (e.g., representativeness errors, etc.). Such methods could be used to tackle classical problems of scale and of related representativeness errors in oceanography such as the link between coarse-scale model or satellite products and in situ "pointwise" observations. Work is presently in progress for the development of validation methodologies of such methods, but we already see in Figures 6a and 6b that the method is able to simulate small-scale structures with at least qualitatively satisfactory levels of variability. Nevertheless, variants of such a method are also possible, for instance improving the point-by-point properties of the cascade with the help of optimal wavelets [*Yahia et al*., 2010]. Physically, progress is needed to simulate realistic filamentary structures required by oceanic applications, which would need additional coupling with a velocity cascade and/or anisotropic cascades.

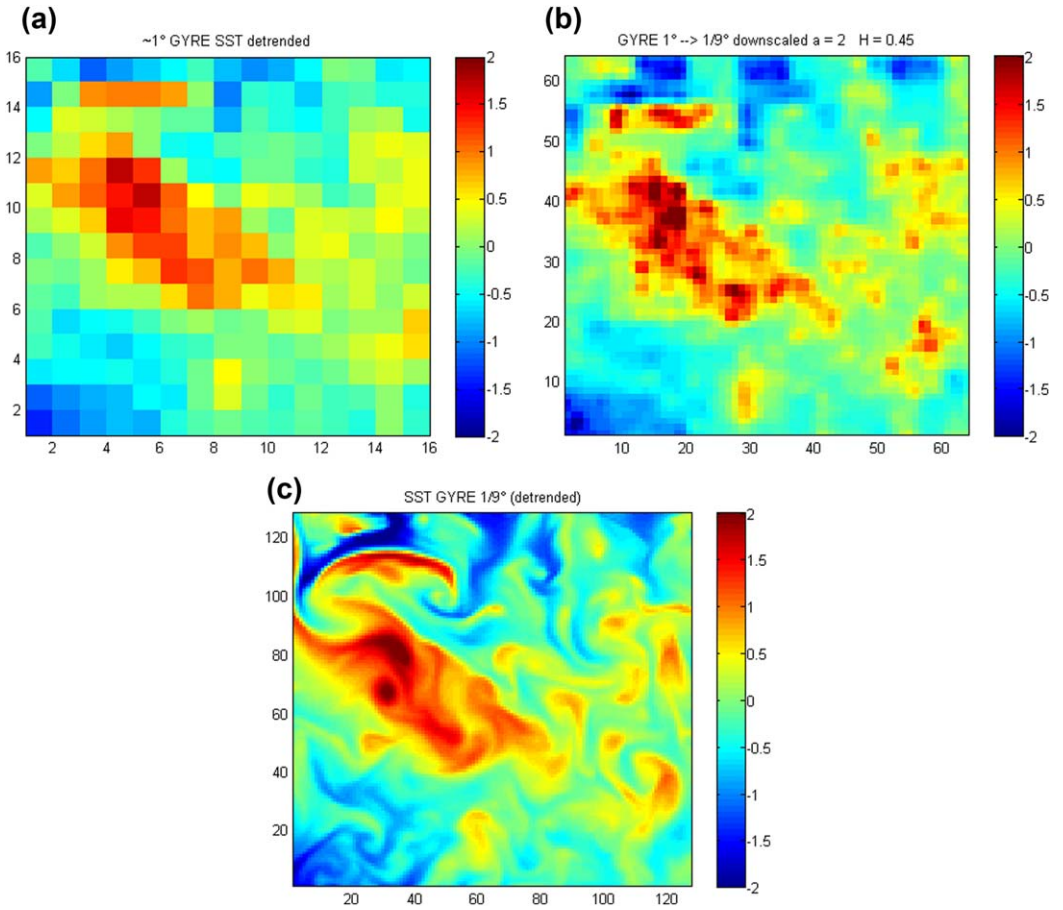

Figure 6. Result of a multifractal downscaling technique for a modeled SST field. (a) An area of a latitudinally detrended SST field produced by NEMO-GYRE at a resolution close to 1° (rigorously, the map is a spatial aggregate at 8/9° of the 1/9° simulation considered in this study). (b) A realization of the higher-resolution field (1/9°) produced by a continuous in scale multifractal downscaling method. (c) The "true" 1/9° simulation used to generate data in Figure 6a. Note that here the downscaling algorithm was calibrated with a single parameter H and does not takes into account possible steeper scaling at very small scales suggested here by Figures 3a–3d. Another limitation is the isotropic hypothesis in multifractal generators, which prevents the downscaled field (Figure 6b) to exhibit proper filamentary structures.

8. Conclusions

Numerous results in the scientific literature based on observational data have shown that the multiscale variability of geophysical fields could be described by scaling, multifractal statistics. Oceanic fields such as surface temperature, salinity, or chlorophyll concentration should obey such statistical constraints. However, multiscale statistical analysis of outputs of numerical models of the ocean was up-to-now restricted to the case of classical second-order statistics such as power spectra. This restriction reduces the description of the statistical properties to a limited range of variability since only the second-order statistics were considered (contrary to multifractal statistics). While recent results have emphasized that numerical models of the atmosphere accurately follow the multifractal laws, it was therefore tempting to evaluate oceanic models in the same way. In the present study, we have applied multifractal analysis tools to outputs of classical, idealized configuration of the NEMO OGCM. While direct structure function analysis of NEMO simulations (in terms of surface temperature, salinity, and velocity) showed the existence of a rupture in the scaling at O(10) times the grid step, possibly due to the an "effective resolution" problem, very different results were found when investigating the statistics of the fluxes (i.e., "gradients" of the state variables) of the simulated quantities. We found evidence of scaling properties for statistics of multiple orders of different (dynamical) surface variables over a significant meso and submesoscale range. These multifractal properties held in almost the whole available scale ranges. While the good scaling properties of the fluxes are associated with the good performance of the NEMO code in terms of probability distributions of turbulent gradients down to scales close to the grid step, the contrasting piecewise scaling property of structure functions

nevertheless suggests that state variables (not the fluxes) remain overfiltered at small scales. The interpretation of this specific scaling break will require subsequent studies in order to determine whether this break is really physical, or is due a filtering of small scales (e.g., related with to the turbulent diffusion scheme), or it is simply an artifact due to the sensitivity of structure function (and spectral) tools to anisotropic features.

As expected from empirical literature results, the fractionally integrated flux is very well suited to describe observed scaling statistics. We found more or less classical α and C1 parameters (respectively, close to 1.8 and 0.1 for most considered variables) with high values of the H (filtering) parameter in the range 0.3–0.8. The present work opens some promising perspectives for modelers. Multifractal analysis tools could be used to evaluate and compare different oceanic models from a multiscale and multi-intensity viewpoint. They are convenient to address classical scale problems in geophysics: e.g., downscaling, calibration of remote sensing instruments based on pointwise data [*de Montera et al*., 2011; *Verrier et al*., 2013]. This is very promising in ocean science since the latter generally deals with two main sources of observational data: coarse-scale satellite data (with a native resolution > 1 km^2, and giving gridded products of much coarser effective resolutions after interpolation and objective analysis) and in situ, pointwise data. Scale representativeness errors are high when trying to merge these different sources of data, and may only be described and corrected with the help of mathematical tools that explicitly take scales and scaling variability into account.

Acknowledgment
S. V. acknowledges the CNES (Centre National d'Etudes Spatiales) for post-doctoral support.

References

Aumont, O., C. Orr, D. Jamous, P. Monfray, G. Marti, and G. Madec (1998), A degradation approach to accelerate simulations to steady-state in a 3-D tracer transport model of the global ocean, *Clim. Dyn.*, *14*(2), 101–116.

Basdevant, C., and R. Sadourny (1983), Modélisation des échelles virtuelles dans la simulation numérique des écoulements turbulents bidimensionnels [published in Special Issue on Two-Dimensional turbulence], *J. Méc. Théor. Appl.*, numero special, 243–269.

Bryan, K. (1969), Climate and ocean circulation. Part 3. Ocean model, *Mon. Weather Rev.*, *97*, 806–827, doi:10.1175/1520-0493(1969).

Capet, X., J. C. McWilliams, M. J. Molemaker, and A. F. Shchepetkin (2008), Mesoscale to submesoscale transition in the California Current System, Part I: Flow structure, eddy flux, and observational tests, *J. Phys. Oceanogr.*, *38*, 29–43, doi:10.1175/2007JPO3671.1.

Charney, J. G. (1971), Geostrophic turbulence, *J. Atmos. Sci.*, *28*, 1087–1095.

Corrsin, S. (1951), On the spectrum of isotropic temperature fluctuations in an isotropic turbulence, *J. Appl. Phys.*, *22*, 469–473.

Currie, W. J. S., and J. C. Roff (2006), Plankton are not passive tracers: Plankton in a turbulent environment, *J. Geophys. Res.*, *111*, C05S07, doi:10.1029/2005JC002967.

de Montera, L., M. Jouini, S. Verrier, S. Thiria, and M. Crepon (2011), Multifractal analysis of oceanic chlorophyll maps remotely sensed from space, *Ocean Sci.*, *7*, 219–229, doi:10.1175/1520-0485(1977)007<0208:NSOTGS>2.0.CO;2.

Deschamps, P. Y., R. Frouin, and L. Wald (1981), Satellite determinations of the mesoscale variability of the sea surface temperature, *J. Phys. Oceanogr.*, *11*, 864–870.

Dubrulle, B. (1994), Intermittency in fully developed turbulence: Log-Poisson statistics and generalized scale covariance, *Phys. Rev. Lett.*, *73*, 959–962.

Gent, P. R., and J. C. Mcwilliams (1990), Isopycnal mixing in ocean circulation models, *J. Phys. Oceanogr.*, *20*, 150–155, doi:10.1175/1520-0485(1990)020<0150:IMIOCM>2.0.CO;2.

Gires, A., I. Tchiguirinskaia, D. Schertzer, and S. Lovejoy (2011), Analyses multifractales et spatio-temporelles des précipitations du modèle Méso-NH et des données radar, *Hydrol. Sci. J.*, *56*(3), 380–396, doi:10.1080/02626667.2011.564174.

Gires, A., C. Onof, C. Maksimovic, D. Schertzer, I. Tchiguirinskaia, and N. Simoes (2012), Quantifying the impact of small scale unmeasured rainfall variability on urban runoff through multifractal downscaling: A case study, *J. Hydrol.*, *442–443*, 117–128, doi:10.1016/j.jhydrol.2012.04.005.

Griffies, S. M., and R. W. Hallberg (2000), Biharmonic friction with a smagorinsky-like viscosity for use in large-scale eddy-permitting ocean models, *Mon. Weather Rev.*, *128*, 2935–2946, doi:10.1175/1520-0493(2000)128<2935:BFWASL>2.0.CO;2.

Hazeleger, W., and S. S. Drijfhout (1998), Mode water variability in a model of the subtropical gyre: Response to anomalous forcing, *J. Phys. Oceanogr.*, *28*, 266–288.

Holladay, C. G., and J. J. O'Brien (1975), Mesoscale variability of sea surface temperatures, *J. Phys. Oceanogr.*, *5*, 761–772, doi:10.1175/1520-0485(1975)005<0761:MVOSST>2.0.CO;2.

Isern-Fontanet, J., A. Turiel, E. García-Ladona, and J. Font (2007), Microcanonical multifractal formalism: Application to the estimation of ocean surface velocities, *J. Geophys. Res.*, *112*, C05024, doi:10.1029/2006JC003878.

Klein, P., et al. (2008), Upper ocean turbulence from high-resolution 3D simulations, *J. Phys. Oceanogr.*, *38*, 1748–1763.

Kolmogorov, A. N. (1941), Local structure of turbulence in an incompressible liquid for very large Reynolds numbers, *Proc. Acad. Sci. URSS Geochem. Sect.*, *30*, 299–303.

Kolmogorov, A. N. (1962), A refinement of previous hypotheses concerning the local structure of turbulence in a viscous incompressible fluid at high Reynolds number, *J. Fluid. Mech.*, *13*, 82–85.

Kraichnan, R. H. (1967), Inertial ranges in two-dimensional turbulence, *Phys. Fluids*, *10*, 1417–1423.

Krauss, W., and R. H. Käse (1984), Mean circulation and eddy kinetic energy in the eastern North Atlantic, *J. Geophys. Res.*, *89*(C3), 3407–3415.

Lapeyre, G., and P. Klein (2006), Dynamics of the upper oceanic layers in terms of surface quasigeostrophy theory, *J. Phys. Oceanogr.*, *36*, 165–176, doi:10.1175/JPO2840.1.

Lavallée, D., S. Lovejoy, D. Schertzer, and P. Ladoy (1993), Nonlinear variability and landscape topography: Analysis and simulation, in *Fractals in Geography*, edited by L. De Cola and N. Lam, pp. 158–192, Prentice Hall, N. Y.

Le Sommer, J., F. d'Ovidio, and G. Madec (2011), Parameterization of subgrid stirring in eddy resolving ocean models. Part 1: Theory and diagnostics, *Ocean Modell.*, *39*, 154–169, doi:10.1016/j.ocemod.2011.03.007.

Le Traon, P. Y., P. Klein, B. L. Hua, and G. Dibarboure (2008), Do altimeter wavenumber spectra agree with the interior or surface quasigeostrophic theory?, *J. Phys. Oceanogr.*, *38*, 1137–1142, doi:10.1175/2007JPO3806.1.
Leith, C. E. (1968), Diffusion approximation for two-dimensional turbulence, *Phys. Fluids*, *11*, 671–673.
Lévy, M., P. Klein, A.-M. Tréguier, D. Iovino, G. Madec, S. Masson, and K. Takahashi (2010), Modifications of gyre circulation by submesoscale physics, *Ocean Modell.*, *34*(1–2), 1–15, doi:10.1016/j.ocemod.2010.04.001.
Lévy, M., L. Resplandy, P. Klein, X. Capet, D. Iovino, and C. Ethé (2012), Grid degradation of submesoscale resolving ocean models: Benefits for offline passive tracer transport, *Ocean Modell.*, *48*, 1–9, doi:10.1016/j.ocemod.2012.02.004.
Lombardo, F., E. Volpi, D. Koutsoyiannis, and S. M. Papalexiou (2013), Just two moments! A cautionary note against use of high-order moments in multifractal models in hydrology, *Hydrol. Earth Syst. Sci. Discuss.*, *10*, 4627–4654, doi:10.5194/hessd-10-4627-2013.
Lovejoy, S., and D. Schertzer (2007), Scale, scaling and multifractals in geophysics: Twenty years on, in *Nonlinear Dynamics in Geophysics*, edited by J. Elsner and A. A. Tsonis, Springer, N. Y.
Lovejoy, S., and D. Schertzer (2010a), On the simulation of continuous in scale universal multifractals, part I: Spatially continuous processes, *Comput. Geosci.*, *36*, 1393–1403, doi:10.1016/j.cageo.2010.04.010.
Lovejoy, S., and D. Schertzer (2010b), On the simulation of continuous in scale universal multifractals, part II: Space-time processes and finite size corrections, *Comput. Geosci.*, *36*, 1404–1413, doi:10.1016/j.cageo.2010.07.001.
Lovejoy, S., and D. Schertzer (2010c), Towards a new synthesis for atmospheric dynamics: Space–time cascades, *Atmos. Res.*, *96*, 1–52, doi:10.1016/j.atmosres.2010.01.004.
Lovejoy, S., and D. Schertzer (2011), Space-time cascades and the scaling of ECMWF reanalyses: Fluxes and fields, *J. Geophys. Res.*, *116*, D14117, doi:10.1029/2011JD015654.
Lovejoy, S., and D. Schertzer (2012), Haar wavelets, fluctuations and structure functions: Convenient choices for geophysics, *Nonlinear Processes Geophys.*, *19*, 1–14, doi:10.5194/npg-19-1-2012.
Lovejoy, S., and D. Schertzer (2013), *The Weather and Climate: Emergent Laws and Multifractal Cascades*, 496 pp., Cambridge Univ. Press, Cambridge, U. K.
Lovejoy, S., D. Schertzer, Y. Tessier, and H. Gaonac'h (2001), Multifractals and resolution independent remote sensing algorithms: The example of ocean colour, *Int. J. Remote Sens.*, *22*, 1191–1234.
Madec, G., and M. Imbard (1996), A global ocean mesh to overcome the North Pole singularity, *Clim. Dyn.*, *12*(6), 381–388.
Madec, G., and The NEMO Team (2008), NEMO ocean engine, in *Note du Pole de Modélisation*, vol. 27, 300 pp., Inst. Pierre-Simon Laplace, Paris.
Madec, G., P. Delecluse, M. Imbard, and C. Lévy (1998), OPA 8.1 ocean general circulation model reference manual, in *Note du Pole de Modélisation*, vol. 11, 91 pp., Inst. Pierre-Simon Laplace, Paris.
Mandelbrot, B. B. (1974), Intermittent turbulence in self-similar cascades: Divergence of high moments and dimension of the carrier, *J. Fluid Mech.*, *62*, 331–350.
Marchesiello, P., X. Capet, C. Menkes, and S. C. Kennan (2011), Submesoscale dynamics in tropical instability waves, *Ocean Modell.*, *39*(1–2), 31–46, doi:10.1016/j.ocemod.2011.04.011.
Meneveau, C., and K. R. Sreenivasan (1987), Simple multifractal cascade model for fully developed turbulence, *Phys. Rev. Lett.*, *59*, 1424–1427.
Muzy, J. F., E. Bacry, and A. Arneodo (1991), Wavelets and multifractal formalism for singular signals: Application to turbulence data, *Phys. Rev. Lett.*, *67*, 3515–3518.
Muzy, J. F., E. Bacry, and A. Arneodo (1993), Multifractal formalism for fractal signals: The structure-function approach versus the wavelet-transform modulus-maxima method, *Phys. Rev. E*, *47*, 875–884.
Nieves, V., C. Llebot, A. Turiel, J. Solé, E. García-Ladona, M. Estrada, and D. Blasco (2007), Common turbulent signature in sea surface temperature and chlorophyll maps, *Geophys. Res. Lett.*, *34*, L23602, doi:10.1029/2007GL030823.
Obukhov, A. (1949), Structure of the temperature field in a turbulent flow, *Izv. Akad. Nauk. SSSR, Ser. Geogr. I Geofiz.*, *13*, 55–69.
Onof, C., and K. Arnbjerg-Nielsen (2009), Quantification of anticipated future changes in high resolution design rainfall for urban areas, *Atmos. Res.*, *92*(3), 350–363, doi:10.1016/j.atmosres.2009.01.014.
Rebora, N., L. Ferraris, J. von Hardenberg, and A. Provenzale (2006), RainFARM: Rainfall downscaling by a filtered autoregressive model, *J. Hydrometeorol.*, *7*, 724–738, doi:10.1175/JHM517.1.
Redi, M. H. (1982), Oceanic isopycnal mixing by coordinate rotation, *J. Phys. Oceanogr.*, *12*, 1154–1158, doi:10.1175/1520-0485(1982)012<1154:OIMBCR>2.0.CO;2.
Reynolds, R. W., and D. B. Chelton (2010), Comparisons of daily sea surface temperature analyses for 2007–08, *J. Clim.*, *23*, 3545–3562, doi:10.1175/2010JCLI3294.1.
Richardson, P. L. (1983), Eddy kinetic energy in the North Atlantic from surface drifters, *J. Geophys. Res.*, *88*(C7), 4355–4367.
Saunders, P. M. (1972), Space and time variability of temperature in the upper ocean, *Deep Sea Res. Oceanogr. Abstr.*, *19*, 467–480.
Schertzer, D., and S. Lovejoy (1987), Physical modelling and analysis of rain and clouds by anisotropic scaling multiplicative processes, *J. Geophys. Res.*, *92*(D8), 9693–9714.
Schertzer, D., and S. Lovejoy (1997), Universal multifractals do exist! Comments on "A statistical analysis of mesoscale rainfall as a random cascade," *J. Appl. Meteorol.*, *36*, 1296–1303.
Schertzer, D., I. Tchiguirinskaia, and S. Lovejoy (2013), Multifractality: At least three moments! Interactive comment on "Just two moments! A cautionary note against use of high-order moments in multifractal models in hydrology" by F. Lombardo et al., *Hydrol. Earth Syst. Sci. Discuss.*, *10*, C3103–C3109.
Semtner, A. J., and Y. Mintz (1977), Numerical simulation of the gulf stream and mid-ocean eddies, *J. Phys. Oceanogr.*, *7*, 208–230.
Seuront, L., F. Schmitt, D. Schertzer, Y. Lagadeuc, and S. Lovejoy (1996a), Multifractal analysis of Eulerian and Lagrangian variability of physical and biological fields in the ocean, *Nonlinear Processes Geophys.*, *3*, 236–246.
Seuront, L., F. Schmitt, Y. Lagadeuc, D. Schertzer, S. Lovejoy, and S. Frontier (1996b), Universal multifractal structure of phytoplankton biomass and temperature in the ocean, *Geophys. Res. Lett.*, *23*(24), 3591–3594.
Seuront, L., F. Schmitt, Y. Lagadeuc, D. Schertzer, and S. Lovejoy (1999), Universal multifractal analysis as a tool to characterize multiscale intermittent patterns: Example of phytoplankton distribution in turbulent coastal waters, *J. Plankton Res.*, *21*, 877–922.
Sharma, D., A. Das Gupta, and M. S. Babel (2007), Spatial disaggregation of bias-corrected GCM precipitation for improved hydrologic simulation: Ping River Basin, Thailand, *Hydrol. Earth Syst. Sci.*, *11*, 1373–1390, doi:10.5194/hess-11-1373-2007.
She, Z.-S., and E. Levesque (1994), Universal scaling laws in fully developed turbulence, *Phys. Rev. Lett.*, *72*, 336.
Skamarock, W. C. (2004), Evaluating mesoscale NWP models using kinetic energy spectra, *Mon. Weather Rev.*, *132*, 3019–3032, doi:10.1175/MWR2830.1.

Smagorinsky, J. (1963), General circulation experiments with the primitive equations, *Mon. Weather Rev.*, *91*(3), 99–164.
Stammer, D. (1997), Global characteristics of ocean variability estimated from regional TOPEX/POSEIDON altimeter measurements, *J. Phys. Oceanogr.*, *27*, 1743–1769, doi:10.1175/1520-0485(1997)027<1743:GCOOVE>2.0.CO;2.
Stolle, J., S. Lovejoy, and D. Schertzer (2009), The stochastic multiplicative cascade structure of deterministic numerical models of the atmosphere, *Nonlin. Processes Geophys.*, *16*, 607–621, doi:10.5194/npg-16-607-2009.
Tessier, Y., S. Lovejoy, and D. Schertzer (1993), Universal multifractals in rain and clouds: Theory and observations, *J. Appl. Meteorol.*, *32*, 223–250.
Turiel, A., J. Solé, V. Nieves, J. Ballabrera-Poy, and E. García-Ladona (2008), Tracking oceanic currents by singularity analysis of microwave sea surface temperature images, *Remote Sens. Environ.*, *112*, 2246–2260, doi:10.1016/j.rse.2007.10.007.
Turiel, A., V. Nieves, E. Garcia-Ladona, J. Font, M.-H. Rio, and G. Larnicol (2009), The multifractal structure of satellite sea surface temperature maps can be used to obtain global maps of streamlines, *Ocean Sci.*, *5*, 447–460.
Umbert, M., N. Hoareau, A. Turiel, and J. Ballabrera-Poy (2014), New blending algorithm to synergize ocean variables: The case of SMOS sea surface salinity maps, *Remote Sens. Environ.*, *146*, 172–187.
Verrier, S. (2011), Modélisation de la variabilité spatiale et temporelle des précipitations par une approche multifractale [in French], PhD thesis, Univ. Versailles St Quentin, Versailles, France.
Verrier, S., L. Barthès, and C. Mallet (2013), Theoretical and empirical scale-dependency of Z-R relationships: Evidence, impacts and correction, *J. Geophys. Res. Atmos.*, *118*, 7435–7449, doi:10.1002/jgrd.50557.
Wyrtki, K., L. Magaard, and J. Hager (1976), Eddy energy in the oceans, *J. Geophys. Res.*, *81*(15), 2641–2646.
Yaglom, A. M. (1966), The influence on the fluctuation in energy dissipation on the shape of turbulent characteristics in the inertial interval, *Sov. Phys. Dokl., Engl. Transl.*, *2*, 26–30.
Yahia, H., J. Sudre, C. Pottier, and V. Garcon (2010), Motion analysis in oceanographic satellite images using multiscale methods and the energy cascade, *Pattern Recognition*, *43*, 3591–3604.